Regenerative Therapy 27 (2024) 365–380

Contents lists available at ScienceDirect

Regenerative Therapy

journal homepage: http://www.elsevier.com/locate/reth

Original Article

Promotive effect of skin precursor-derived Schwann cells on brachial plexus neurotomy and motor neuron damage repair through milieu-regulating secretome

Jia-nan Chen [a, b, 1], Xiao-jia Yang [a, c, 1], Meng Cong [c], Ling-jie Zhu [a, c], Xia Wu [c], Li-ting Wang [a, c], Lei Sha [a], Yan Yu [a, c], Qian-ru He [c], Fei Ding [c], Hua Xian [a, d, **], Hai-yan Shi [a, c, *]

[a] School of Medicine, Nantong University, Nantong, 226001, China
[b] Department of Pediatric Surgery, The First Affiliated Hospital of Nanjing Medical University, Nanjing, 210029, China
[c] Key Laboratory of Neuroregeneration of Jiangsu and Ministry of Education and Co-innovation Center of Neuroregeneration, Nantong University, Nantong, 226001, China
[d] Department of Pediatric Surgery, Affiliated Hospital of Nantong University, Nantong University, Nantong, 226001, China

ARTICLE INFO

Article history:
Received 28 August 2023
Received in revised form
2 April 2024
Accepted 11 April 2024

Keywords:
Skin precursor-derived Schwann cells
Branchial plexus injury
Secretome
Motor neurons
Regenerative microenvironment
Hypoxia-responsive cytokines

ABSTRACT

Brachial plexus injury (BPI) with motor neurons (MNs) damage still remain poor recovery in preclinical research and clinical therapy, while cell-based therapy approaches emerged as novel strategies. Previous work of rat skin precursor-derived Schwann cells (SKP–SCs) provided substantial foundation for repairing peripheral nerve injury (PNI). Given that, our present work focused on exploring the repair efficacy and possible mechanisms of SKP-SCs implantation on rat BPI combined with neurorrhaphy post-neurotomy. Results indicated the significant locomotive and sensory function recovery, with improved morphological remodeling of regenerated nerves and angiogenesis, as well as amelioration of target muscles atrophy and motor endplate degeneration. Besides, MNs could restore from oxygen-glucose-deprivation (OGD) injury upon SKP-SCs-sourced secretome treatment, implying the underlying paracrine mechanisms. Moreover, rat cytokine array assay detected 67 cytokines from SKP-SC-secretome, and bioinformatic analyses of screened 32 cytokines presented multiple functional clusters covering diverse cell types, including inflammatory cells, Schwann cells, vascular endothelial cells (VECs), neurons, and SKP-SCs themselves, relating distinct biological processes to nerve regeneration. Especially, a panel of hypoxia-responsive cytokines (HRCK), can participate into multicellular biological process regulation for permissive regeneration milieu, which underscored the benefits of SKP-SCs and sourced secretome, facilitating the chorus of nerve regenerative microenvironment. Furthermore, platelet-derived growth factor-AA (PDGF-AA) and vascular endothelial growth factor-A (VEGF-A) were outstanding cytokines involved with nerve regenerative microenvironment regulating, with significantly elevated mRNA expression level in hypoxia-responsive SKP-SCs. Altogether, through recapitulating the implanted SKP-SCs and derived secretome as niche sensor and paracrine transmitters respectively, HRCK would be further excavated as molecular underpinning of the neural recuperative mechanizations for efficient cell therapy; meanwhile, the analysis paradigm in this study validated and anticipated the actions and mechanisms of SKP-SCs on traumatic BPI repair, and was beneficial to identify promising bioactive molecule cocktail and signaling targets for cell-free therapy strategy on neural repair and regeneration.

Abbreviations: α-BTX, α-bungarotoxin; BPI, brachial plexus injury; CMAP, compound muscle action potential; CM, conditioned medium; EVs, extracellular vesicles; HRCK, hypoxia-responsive cytokines; MNs, motor neurons; LBPI, lower brachial plexus injury; OGD, oxygen and glucose deprivation; PNI, peripheral nerve injury; SKP-SCs, Schwann cells derived from skin precursors; SKPs, skin-derived precursors; TGT, Terzis grooming test.

* Corresponding author. School of Medicine, Nantong University, Nantong, 226001, China.
** Corresponding author. Department of Pediatric Surgery, Affiliated Hospital of Nantong University, Nantong University, Nantong, 226001, China.
E-mail addresses: xianhua@ntu.edu.cn (H. Xian), haiyansh@ntu.edu.cn (H.-y. Shi).
Peer review under responsibility of the Japanese Society for Regenerative Medicine.
[1] Jia-nan Chen and Xiao-jia Yang have contributed equally to this work.

https://doi.org/10.1016/j.reth.2024.04.002

1. Introduction

Brachial plexus injury (BPI) is a common and frequently-occurring clinical problem belong to peripheral nerve injury (PNI), the incidence of which has been on the rise in recent years. Usually, traumatic BPI is caused by cervical spine procedures, industrial injury, traffic accident, or birth injury [1]. Anatomically brachial plexus can be divided into five sections: roots, trunks, division, cords and terminal branches, and ends with five terminal branches, including upper limb innervation, musculocutaneous, median nerve, axillary nerve, radial and ulnar nerve [2]. Given the sensatory and locomotive function of brachial plexus in the upper extremities, shoulder and back, and chest, once occur BPI, the patient would suffer from partial or complete loss of upper limb function, even leaving them with lifelong disability [1]. BPI can be divided into the upper trunk injury, extended upper trunk injury, lower trunk injury, and swinging hand with all roots injury involved [2], including preganglionic and postganglionic BPI [3]. Consequently, the therapy for BPI is still in challenge that depends on the type of BPI and the approach strategy development [4].

It has been recognized that patients with lower trunk injury often lose most of their target muscles functions, especially paralysis of the flexion muscle of the arm, impairment of finger flexion, and incapacitation of the intrinsic muscles of the hand [4]. Moreover, researcher reported that following lesion of peripheral nerve in mammals, motor neurons (MNs) underwent a cell death, the significant MNs loss causing the paralysis of the target muscle groups [5,6]. There have been fewer approaches for the repair of injuries to the brachial plexus lower trunk, which mainly include intercostal nerve, phrenic nerve or contralateral C7 nerve transfer, the curative effect was remain poor with worse muscle force recovery [7]. Despite recent work combined an electroencephalography-based human–machine interface with the classic contralateral C7 nerve transfer operation approach, motor cortical remodeling was still a vital toughie for BPI repair [8]. Therefore, it is urgent to seeking novel therapeutic modalities to help reconstruct the neural and muscular morphology and function quickly and effectively.

Due to all movements are modulated by the activation of MNs [9], the severity and regenerative capacity of the injured MNs after PNI were the key element to improve functional recovery, and maintaining the survival of affected MNs is extremely essential for axonal regeneration. The advances of intervention strategies in promoting MN activity mainly contained small molecules [10], neurotrophic factors [11], stem cell implantation [12], stem cell-derived neurons implantation [13], and stem cell-sourced secretome [14]. Upon stem cell-based therapy, to sustain neuronal survival and axonal outgrowth, exogenous cells may interact with various endogenous cells through paracrine cytokines after implantation to promote nerve regeneration. Notably, these paracrine bioactive factors might have similar or different regulatory potency on distinct cell types, covering Schwann cells, vascular endothelial cells, neurons, inflammatory cells and implanted cells themselves, involved in orchestrating the neural regeneration microenvironment [15]. Currently, cell secretome components has emerged as a novel therapeutic strategy for the treatment of neuropathy [16].

For PNI repair, Schwann cell application was well-known as the gold criteria of cell-based therapy [17,18]. Due to the scarcity of native Schwann cells at injury spot, prompting damage to other nerves for sufficient autologous cells [19], alternative Schwann-like cells originated from abundant stem cells as novel sources is an emerging consensus and worthy to be extensively applied and deeply delineated. Given that, rodents and human skin-derived precursors (SKPs) as self-renewing and pluripotent adult stem cells, can provide sufficient source of Schwann-like cells [20], that attracted our attention. Previous works have evidenced that Schwann cells derived from skin precursors (SKP–SCs) presented neuroprotection for the injured and dysmyelinated nervous system [21], improving behavioral function recovery after acute or chronic sciatic nerve injury [22], myelination capacity in demyelinated focal tibial nerve [23], and sensory recovery after PNI [24]. SKP-SCs might promote nerve regeneration via immunomodulatory properties [25], nevertheless, the underlying action mechanisms of SKP-SCs on boosting peripheral neural regeneration are still remain to be further uncovered.

Aim to validate the effects of rat SKP-SCs treatment on rat traumatic BPI and damaged MNs, a transected model of the lower trunk of branchial plexus in rats was established. Then the in vitro expanded SKP-SCs were injected to the damaged nerve post-stumps-coaptation. Functional evaluations were performed through the recovery period, and morphometric analysis of nerve and muscle were used to assess the efficacy. Meanwhile, MNs from the fetal rats were obtained and cultured to simulate a damaged model via oxygen and glucose deprivation (OGD) procedure, then neuronal morphology observation and cell viability assay were performed to prove the therapeutic potential of SKP-SCs-sourced conditioned medium (SKP-SC-CM) on injurious MNs.

Moreover, cytokines as bioactive factors can be directed released into secretome, namely soluble cytokines, also may be encapsulated into extracellular vesicles (EVs). Since EVs and secretome both can be utilized as cell-free therapeutic strategies [16], more recently, our studies revealed the EVs derived from SKP-SCs processing desirable efficacy of enforcing the cell viability and neurite regrowth of OGD- or axotomy-damaged neurons [26,27]. Thereby here we focused on soluble molecules in secretome, in spite of the previous findings demonstrated that SKP-SC-CM could provide neuroprotective effect on neurons through inhibiting apoptosis and regulating autophagy by PI3K/AKT pathway [28,29], and insulin-like growth factor-2 (IGF-2) was screened out as an useful target for Parkinson's disease treatment via mass spectrometry analysis [28,30], the other bioactive factors such as crucial cytokines and chemokines in SKP-SC-secretome remained unclear. On this basis, a protocol named cytokine array assay and corresponding bioinformatics analysis was subjected to further explore the cytokines in SKP-SCs-sourced secretome, revealing the underlying molecular reparative mechanisms and possible microenvironment regulation paradigm.

2. Materials and methods

2.1. Culture and characterization of SKP-SCs

In our previous work, the primary rat SKP-SCs were obtained and cryopreserved at early passages [26]. Here, the cell resuscitation and expansion of SKP-SCs were performed for experimental application. The proliferating SKP-SCs were cultured in Schwann cell proliferation medium, namely DMEM/F12 medium (Corning, Manassas, VA, USA) containing 1% penicillin/streptomycin (Beyotime, Shanghai, China), 5 μm forskolin (Sigma–Aldrich, St Louis, MO, USA), 50 ng/mL heregulin-1β (R&D, Minneapolis, MN, USA), 2% N2 supplement (StemCell Technologies, Vancouver, BC, Canada), and 1–5% fetal bovine serum (FBS) (Sigma–Aldrich).

The identification of SKP-SCs were performed via immunocytochemistry staining with rabbit anti-S100β antibody (1:400, Invitrogen, Thermo Fisher Scientific, Rochester, MN, USA) and chicken-anti-glial fibrillary acidic protein (GFAP) antibody (1:1000, Abcam, Cambridge, UK) respectively at 4 °C overnight, followed by reaction with secondary antibody of goat anti-rabbit-IgM-Cy3 (1:400, Abcam) and donkey anti chicken IgG-fluorescein

isothiocyanate (FITC) (1:400, Abcam) at 25 °C for 2 h, then cells were counterstained with Hoechst 33258. Images were captured by Confocal Microscope.

2.2. Animal surgical procedures and grouping schemes

In this study, the lower brachial plexus injury (LBPI) model was performed in adult male SD rats (8 weeks old, weighing 220–240 g), animals were obtained from the Laboratory Animal Services Centre of Nantong University. Total 30 animals were divided randomly into three groups: sham group, phosphate buffer saline (PBS) group and SKP-SC group. For each group 10 rats were used to perform the behavioral test and the electrophysiological examination, and the nerve and target muscle morphologic observation, as well as nerve myelination structure observation. Rats were anesthetized by intraperitoneal injection with 3% pentobarbital sodium (Sigma–Aldrich) (30 mg/kg). In sham group, a skin incision (2–3 cm) along the lower edge of the right clavicle was made slightly, then the skin incision was sutured by 5–0 suture needle. In the other two groups, the right branchial plexus, including medium trunk and inferior trunk, was exposed after bluntly separating the covered muscles; then the inferior trunk was separated and transected, followed by coaptation using 8-0 microsuture; next, 5 μl cell suspension (about 2×10^{10} cells) or PBS was injected into epineurium in distal site 5 mm close to the axotomy respectively; finally, the skin incision was sutured the same as that in sham group. All the animal experimental procedures according to the Institutional Animal Care Guidelines of Nantong University were approved by the Jiangsu Provincial Administration Committee of Experimental Animals (No. 20150305–030), and ethically approved by the Laboratory Animal Center of Nantong University (No. IACUC202202151005) on February 15, 2022.

2.3. Motor and sensory behavior test

Following surgery, we performed the Terzis grooming test (TGT) weekly to evaluate the motor function of the upper limbs [31]. Each rat was placed in a spacious and quiet environment, 3–5 ml bacteria-free water was sprayed on the nose of the experimental rat with a 10-mL syringe to induce bilateral grooming behavior of the upper limbs. A 0–5 rating scale was utilized depending on the highest position where the affected forelimb could reach. Grading systems of 0–5 are as follows: 0, no response; 1, elbow flexion but unable to reach the nose; 2, elbow flexion reaching the nose; 3, reaching below the eyes; 4, reaching the eyes; 5, reaching the ear or beyond. Meanwhile, the cold sensitivity was measured by an acetone evaporation test as described previously [32]. After the acetone (250 μl) was squirted onto the mid-plantar surface of the right forepaw, the withdrawal responses were evaluated on a scale of 0–3 points: 0, the paw was not moved; 1, a response in which the paw had little or no weight on it; 2, a response in which the paw was elevated and was not in contact with any surface; 3, a vigorous response in which the rat licked, bit or shook the paw. The test to each rat was repeated for not less than 3 times, and the internal of each time not less than 15 min.

2.4. Electrophysiological evaluation of biceps muscles

At 6 weeks postoperatively, rats were subjected to electrophysiological examinations in each group. By incision, the regenerated brachial plexus was re-exposed under anesthesia, and the compound muscle action potential (CMAP) was recorded using a Keypoint 2 portable electromyography system (Dantec, Copenhagen, Denmark). The brachial plexus was stimulated at the distal end of the injury site by electric stimuli with a hook electrode, and a monopolar needle recording electrode was inserted in the biceps mid-melly muscle. Supramaximal stimulation (with an intensity of 1 mA) was given to evoke the maximum CMAP response. The amplitude of CMAP was recorded for each rat.

2.5. Morphologic observation of nerves

Six weeks postoperatively, to assess the regeneration of nerve and neurovascular bundles, rats were deeply anesthetized with an overdose of pentobarbital sodium (100 mg/kg, i.p.) and then perfused transcardially with PBS followed with 4% paraformaldehyde. The regenerated brachial plexus of rats was excised, routinely post-fixed and dehydrated by gradient sucrose. Then the 12 μm thick longitudinal or cross-sectional sections of nerve were cut by Cryostat (CM3050S, Leica, Mannheim, Germany), then were incubated with primary antibodies respectively overnight at 4 °C, including mouse anti-neurofilament 200 (NF200) (1:400, sigma-Aldrich), mouse anti-S100β (1:400, Abcam, Cambridge, UK), and rabbit anti-CD31, followed by incubating with the secondary antibody at room temperature for 2 h, including goat anti mouse IgG 488 (1:400, Jackson, West Grove, PA, USA), goat anti mouse IgG Cy3 (1:400, Jackson), and goat anti-rabbit-IgM-Cy3 (1:200, Abcam). All above sections were counterstained with Hoechst 33258 (Abcam). The samples were observed under the Confocal Microscope (TCS SP5, Leica, Mannheim, Germany) and the fluorescent microscope (Axio Imager M2, Zeiss, Oberkochen, Germany). And the captured images were quantitatively analyzed by using Image J software (version 1.8.0; National Institutes of Health, Bethesda, MD, USA).

To investigate the nerve remyelination, 5 mm long nerve segments distal to the injury site were post-fixed and stained with lead citrate and uranyl acetate, followed by observation under Transmission Electron Microscopy (TEM) (Hitachi, Tokyo, Japan). And images were taken from random fields of each section to measure the thickness of myelin sheaths, the diameter of myelinated nerve fibers, and the number of myelin sheath lamellar using Image J software.

2.6. Morphometric analysis of muscles

Similar to the above, both ipsilateral and contralateral target biceps muscles were collected and weighed, then the ipsilateral/contralateral wet weight ratio was calculated. Next, the muscles were post-fixed, and dehydrated by sucrose, then cut into 12 μm thick transverse sections with Cryostat. The samples were reacted with the primary anti-laminin antibody (1:500) (Abcam) and secondary FITC-anti-rabbit-IgM antibody (1:400) (Proteintech, Wuhan, Hubei, China). After counterstaining with Hoechst 33258, the fluorescent photos were taken to be analyzed by Image J software. Moreover, for evaluating the neuromuscular junction, 12-μm thick longitudinal muscle sections were directly co-stained with α-bungarotoxin (α-BTX) (1:220) (Sigma–Aldrich) at room temperature for 2 h in dark, and images of motor endplates were captured by the Confocal Microscope.

Besides, the post-fixed muscle samples were dehydrated by gradient ethanol at 4 °C, and embedded in paraffin blocks. The prepared 5 μm transverse tissue sections were deparaffinized, and subjected to Masson's trichrome staining according to the kit instructions (Solarbio, Beijing, China). The muscle images were taken under the Light Microscope (Axio Imager M2, Zeiss, Oberkochen, Germany). Using Image J software, the percentage area of muscle fiber and collagen fiber in gross morphology were measured; in random fields of view, the mean cross-sectional area of muscle fibers and the average percentage of collagen fiber area were further measured.

2.7. Culture and identification of MNs

To obtain MNs, on gestation day 13.5 a pregnant rat was isoflurane anesthetized, and sacrificed via cervical dislocation, and the fetal rats were removed from the uterus. The spinal cord of fetal rats soaked in Leibovitz's L-15 medium (Gibco, Carlsbad, CA, USA) was separated, then digested with 0.125% trypsin at 37 °C for 30 min. The purification of the MNs was performed in 15% OptiPrep gradient centrifugation solution (Sigma–Aldrich, St. Louis, MO, USA). Finally, the primary single cell suspension was obtained, and cultured on Poly-L-lysine (PLL) (Sigma–Aldrich) coated plates in DMEM medium (Corning) containing 1% penicillin/streptomycin and 10% FBS for 4 h. Next, culture medium changed to the ™Neurobasal medium (Gibco) containing 2% B27 (Gibco), 1% glutamine (Gibco) and 1% penicillin/streptomycin (Beyotime, Shanghai, China), and refreshed every other day.

In order to identify MNs, the primary antibody of chicken anti-choline acetyltransferase (ChAT) (1:200, Abcam) and mouse anti-β-tubulin III (TUJ1) (1:600, Abcam) were incubated with neurons at 4 °C overnight, followed by reaction with secondary antibody of goat anti mouse IgG-Cy3 (1:600, Jackson) and donkey anti chicken IgG-fluorescein isothiocyanate (FITC) (1:400, Abcam) at 25 °C for 2 h, then neurons were counterstained with Hoechst 33258. Images were captured by Confocal Microscope.

2.8. Treatment of OGD-injured MNs with SKP-SC-CM

SKP-SCs were seeded on the dishes coated with Poly-D-lysine (PDL) (Sigma–Aldrich)-Laminin (Corning). At about 80% cell confluence after culture, medium was switched to serum-free medium for another 48 h. The supernatant, namely SKP-SC-CM, was collected and went through sequential ultracentrifugation 800 g for 10 min at 4 °C to remove the cell debris. Next, to obtain the 20 times concentrate supernatants, the SKP-SCs supernatants was added to the concentrated filter column (Amicon Ultra-15 Centrifugal Filter Devices, washing by sterilized Milli-Q water twice) and centrifuged with 3000 g for 20 min at 25 °C.

In order to establish an OGD-injured model of MNs, after inoculating for 4 days, the primary cultured neurons were washed twice by Neurobasal™-A medium (Gibco), then cultured in Neurobasal™-A medium (Gibco), containing 2% B27, 1% glutamax, and 1% penicillin/streptomycin, in 37 °C incubator with 5% CO_2 and 1% oxygen concentration for 1 h. Then the cultures were switched back into the Neurobasal™ medium with or without the SKP-SC-CM, and cultured in the normal incubator for 24 h. The control group was treated with the routine exchange of the cell medium every other day.

2.9. Neuronal morphology observation and cell viability assay

To detect the effect of SKP-SC-CM on the cell viability of OGD-injured neurons, MNs were inoculated into 96-well plates in density of 10^5/well. After OGD for 1 h, neurons were switched to normal culture condition for 24 h, added 1.25%, 2.5%, 5%, 10% or 20% SKP-SC-CM to medium respectively according to the concentration gradient groups. The neuronal cell viability was assessed with tetrazolium salt reduction assay by Cell counting kit-8 (CCK8) (Dojindo, Kumomoto, Japan) assay. In short, CCK8 solution at a 10:1 ratio was added into different groups of 96-well plates (6 wells each group), and incubated at 37 °C for 4 h. The value of optical density was measured at 450 nm by Microplate Reader (BioTek, Burlington, VT, USA). The results were expressed as a percentage value relative to the control group.

Meanwhile, OGD-injured MNs inoculated on 24-well plates were treated with 20% SKP-SC-CM for 24 h. Then TUJ1 immunofluorescence staining was performed, neurons were observed, and fluorescence photographs were taken randomly. The average length of the longest neurites and the average branch numbers of neurites were counted for not less than 100 neurons in each group by Image J software.

2.10. Cytokine array assay and analysis of SKP-SC-sourced secretome

Firstly, the cytokines secreted from SKP-SCs was tested by Rat Cytokine Array GS67 (RayBiotech, Guangzhou, China) following the manufacturer's instructions. According to the expression abundance results, cytokines that with greater expression abundance (more than 1000 Mean signal values) were screened out from the primary data. Then, the biological processes of gene ontology (GO) annotations of each cytokine (Rattus Norvegicus) was downloaded from the UniProt Database (http://www.uniprot.org).

Secondly, the associated cell types involved in nerve regeneration microenvironment was designated, including neurons, Schwann cells, vascular endothelial cells (VECs), inflammatory cells, and the implanted SKP-SCs. Several crucial medical subject headings (MESH) and expanded corresponding annotation terms used for searching were confined on the basis of the different cellular biological functions or response activities of each cell type respectively.

Thirdly, the various cytokines were further analyzed to confirm whether any annotated biological process was relevant to any MESH. If necessary, the result would be further determined by searching relevant literature. The retrieved cytokines and annotations were finally conducted enrichment analysis, forming the tables of the data set.

Finally, the GO clusters of the classified candidate cytokines were displayed via scatter plot; then the associated cytokine number to each cellular MESH, and the relevant cell type number to each cytokine were showed by aggregated numbers in histograms.

2.11. Quantitative reverse transcriptase-polymerase chain reaction (qRT-PCR)

Total RNA was isolated from SKP-SCs using Trizol reagent (Sigma), and cDNA was obtained using HiScript ® III 1st Strand cDNA Synthesis Kit (Vazyme, Nanjing, China) according to the manufacturer's instructions. qRT-PCR was performed with Taq Pro Universal SYBR qPCR Master Mix (Vazyme) on the BIO-RAD system (BIO-RAD-96CFX) according to standard methods. The mRNA expression of nine cytokines in normoxia SKP-SCs and hypoxia SKP-SCs were detected. The primer sequences for each gene are described in Table 1. The expression of actin was used for standardization. The results were analyzed by the $2^{-\triangle\triangle Ct}$ method.

2.12. Statistical analysis

Statistical analyses were performed using GraphPad Prism 8.0.1 software (GraphPad Prism Software Inc, San Diego, CA, USA). All data are presented as means ± SEM. One-way ANOVA followed by Tukey's multiple comparisons test for multiple comparisons, p value < 0.05 was considered to be statistically significant.

3. Results

3.1. Morphology of SKP-SCs

The resuscitated SKP-SCs remained the typical morphology in passage culture, with a bipolar spindle-shape and strong refractivity of the cell body, as well as the side by side alignment along

the longitudinal axis (Fig. 1A). Meanwhile, immunofluorescence staining results demonstrated the positive co-expression of Schwann cell associated marker proteins S100β and GFAP in SKP-SCs, based on the purity identification, cells were used in following experiments (Fig. 1B).

3.2. Anatomical morphology of brachial plexus in Sprague Dawley rats compared to that in Wistar rats

To construct an appropriate operation approach and route for BPI in Sprague Dawley (SD) rats, we first contrasted the anatomy morphology of brachial plexus in SD rats and Wistar rats [33]. The morphology of branchial plexus in SD rats was shown after removal of clavicle and covered muscles through our dissection operation (Fig. 1C), the same as that in Wistar rats [33], branchial plexus is divided into the truncus superior (TS) composed of C5 and C6, the C7 formed truncus medius (TM), and the truncus inferior (TI) composed of C8 and T1. However, the location of C5 and C6 of branchial plexus was too deeper to expose via operation under clavicle in SD rats, based on maintaining the normal cervical skeletal muscle system structure and function. Accordingly, a separating and transecting injury model of the lower brachial plexus in SD rats was feasibly established in present work, and following coaptation the SKP-SCs implantation was performed to treat the inferior trunk injury (Fig. 1D).

3.3. SKP-SC treatment enhanced the functional recovery of upper limb

The recovery of motor function in rat upper limb was evaluated using TGT weekly. Before surgery, all the animals displayed normal elbow flexion with a mean score of 5. All the injured groups had a score of 0 at 24 h post-injury indicating a total loss of motor function and proved a successful surgical operation of BPI. Functional recovery was initially observed from the first week after surgery and the scores increased from week to week in all surgical groups. Moreover, the average scores in SKP-SC treated group were remarkably improved when compared with the PBS treated group (Fig. 2A). At 6 weeks after surgery, there were two rats with a score of 5 in the SKP-SC group, while no rats in the PBS group reached this level.

Besides, the cold sensitivity evaluation result was similar to the motor function recovery trend. In short, the recovery of rat response to acetone stimuli improved gradually, and the score of SKP-SC group was significantly better than the score of PBS group. More obviously, at week 4 after operation, all rats in SKP-SC group reached full score (Fig. 2B).

To further confirm the function recovery, animals were subjected to the electrophysiological assessments 6 weeks after surgery, presented the CMAP at the distal end of brachial plexus interior trunk. Compared with that in the PBS group, the CMAP amplitudes in SKP-SC and sham groups were significantly higher (Fig. 2C). Altogether, SKP-SC treatment contributed to a better functional recovery of BPI than PBS control.

3.4. SKP-SC treatment facilitated nerve regeneration

According to the immunohistochemistry (IHC) staining results of the longitudinal nerve frozen sections, it was showed that the fluorescence expression intensity of NF200 and S100β in PBS group was significantly decreased compared with that in sham group, while the expression of SKP-SC group was significantly increased compared with PBS group (Fig. 3A,B,C). It was demonstrated that the outgrowth of nerve was improved and the proliferated Schwann-like cells facilitated to the regeneration.

Moreover, the expression of CD31 in PBS group was lower than that in sham group, while that was higher in SKP-SC group than in PBS group, according to the immunostaining results of the Cross-sectional nerve frozen sections (Fig. 3D), suggesting that the pro-neuroregeneration effect of SKP-SCs was in agreements with the pro-angiogenesis effect.

Furthermore, the ultrastructure of regenerated nerve fibers was observed under TEM. The significantly regenerated nerve fibers were presented, and the myelinated axons were surrounded by thick and electron-dense myelin sheaths with clear lamellas (Fig. 4A). The statistical analysis of three indicators, the diameter of the myelinated nerve fibers, the thickness of myelin sheath, and the number of myelin lamellas in each group, showed significant decrease in PBS group compared with that in sham group, while markedly increase in SKP-SC group compared with that in PBS group (Fig. 4B,C,D). To sum up, above results indicated that injecting SKP-SCs into injured branchial plexus can promote the remyelination of the regenerated nerves.

3.5. SKP-SC treatment alleviated muscle atrophy

The neuromuscular system plays an important role in the process of movement. After nerve injury, muscular atrophy will be induced by denervation. To a certain extent, the muscle recovery depends on the nerve regeneration and reinnervation. We assessed the biceps muscles change among different groups to examine the repair effect of SKP-SCs on target muscle after BPI. First, results showed that, except for sham group, biceps muscles at the injured side displayed obvious atrophy compared with that at the contralateral side (Fig. 5A). The wet weight ratio of target muscles in SKP-SC group was significantly higher than that in PBS group, despite slightly lower than that in sham group (Fig. 5B). Through Masson's trichrome staining, the percentage of muscle fibers in the gross morphology were statistically analyzed, showing lower percentage in PBS group than that in sham group, and higher percentage in SKP-SC group than that in PBS group, while collagen percentage showing opposite results (Fig. 5C,D,E). With respect to the mean

Table 1
Primer sequences for qRT-PCR.

Gene name	Protein name	Sense Primer Sequence (5′ to 3′)	Anti-Sense Primer Sequence (5′ to 3′)
actin	Actin	TGTCACCAACTGGGACGATA	GGGGTGTTGAAGGTCTCAAA
Cx3cl1	Fractalkine	TCCAAAGCTCAGGATGCAGG	AGTAGCTTTTTCCTCGGCCC
Icam1	ICAM-1	CGCCAGAGGAAGATCAGGAT	AGGTGGGTGAGGGGTAAATG
Il1a	IL-1α	AGCCTGTGTTGCTGAAGGAGATTC	CTCTGGGAAAGCTGCGGATGTG
Il1b	IL-1β	AGTTGACGGACCCAAAAG	AGCTGGATGCTCTCATCAGG
Ccl2	MCP-1α	TGCTGCTACTCATTCACTGGC	CCTTATTGGGGTCAGCACAG
Pdgfaa	PDGF-AA	GCCATTCCCGCAGTTTG	GGCTGGCACTTGACGCT
Tnfa	TNF-α	CGTCGTAGCAAACCACCAAGC	CCAGTCGCCTCACAGAGCAAT
Vegfa	VEGF-A	TCAGGAGGACCTTGTGTGATC	CATTGCTCTGTACCTTGGGAA
Nothch1	Notch1	GCAGCCACAGAACTTACAAATCCAG	TAAATGCCTCTGGAATGTGGGTGAT

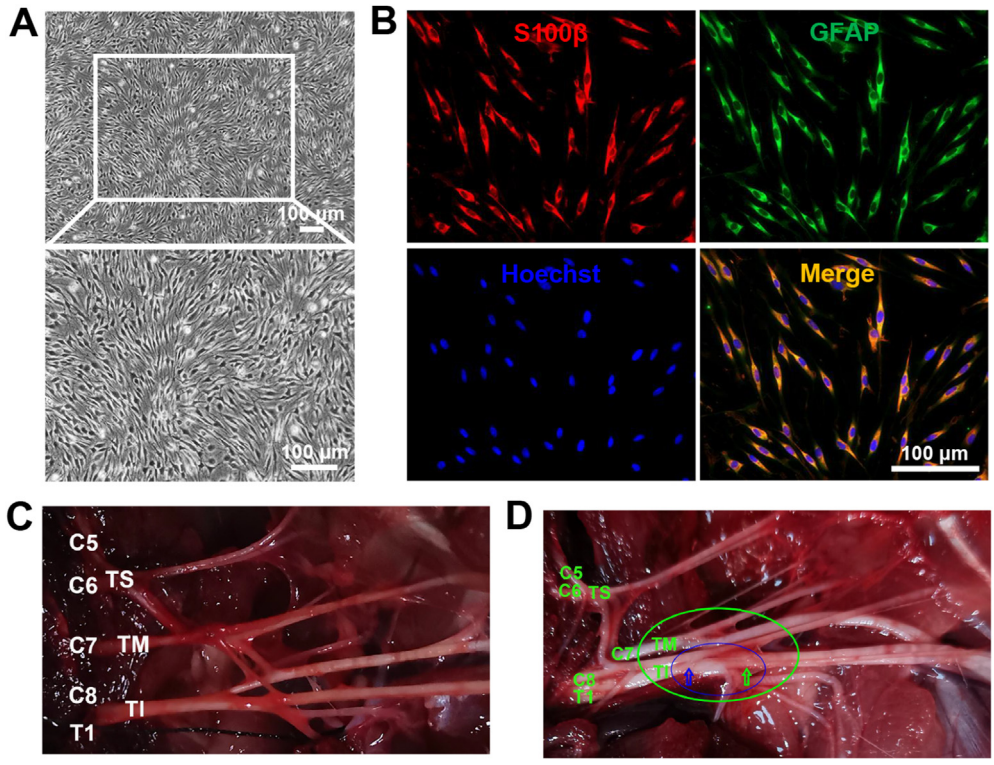

Fig. 1. Identification of rat SKP-SCs and cell implantation treatment to lower brachial plexus injury (LBPI). (A, B) SKP-SCs showed a typical bipolar spindle-shape with side by side alignment. Immuno-stained SKP-SCs positively expressed Schwann cell markers S100β (red) and GFAP (green), with DAPI stained cell nuclei (blue). Scale bar, 100 μm. (C) Anatomic morphology of branchial plexus in Sprague–Dawley rats. (D) Photograph showing the operative region at inferior trunk of branchial plexus, the green and blue circle represented the exposed surgical field and the damaging position respectively, the blue and green arrow represented the transection injury location and cell injection point respectively.

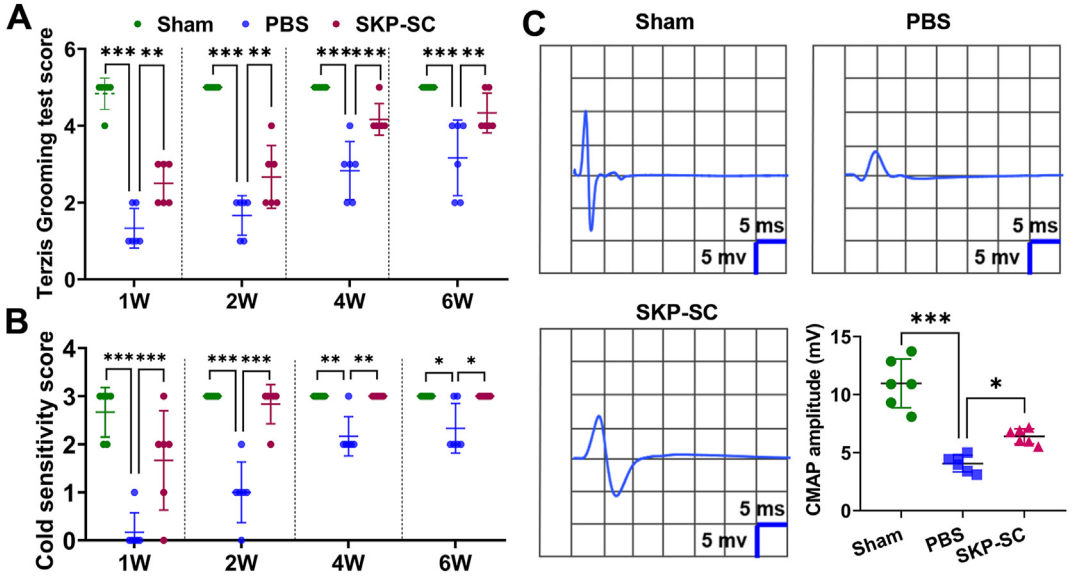

Fig. 2. Functional recovery evaluation of regenerated nerves. (A, B) Evaluation of Terzis grooming test score and cold sensitivity score increased with time by week, showing significant recovery in SKP-SC group than in PBS group in six weeks. (C) Representative electrophysiological CMAP curves of the injured side at six weeks after surgery, the significance difference of CMAP amplitudes was statistically analyzed. Data are presented as Mean ± SEM, $n = 6$; *, $p < 0.05$; **, $p < 0.01$; ***, $p < 0.001$.

cross-sectional area of muscle fibers, that in PBS group was significantly reduced compared with Sham group, while in SKP-SC group muscle atrophy was significantly ameliorated compared with PBS group, by detecting stained paraffin section in each group. In addition, in agreement to the gross morphology, the average percentage of collagen in PBS group presented significant increase compared with that in sham group, while that in SKP-SC group decreased markedly compared with that in PBS group (Fig. 5F,G,H).

Second, the morphological changes of muscle fibers were evaluated using laminin immunostaining in frozen transverse muscle

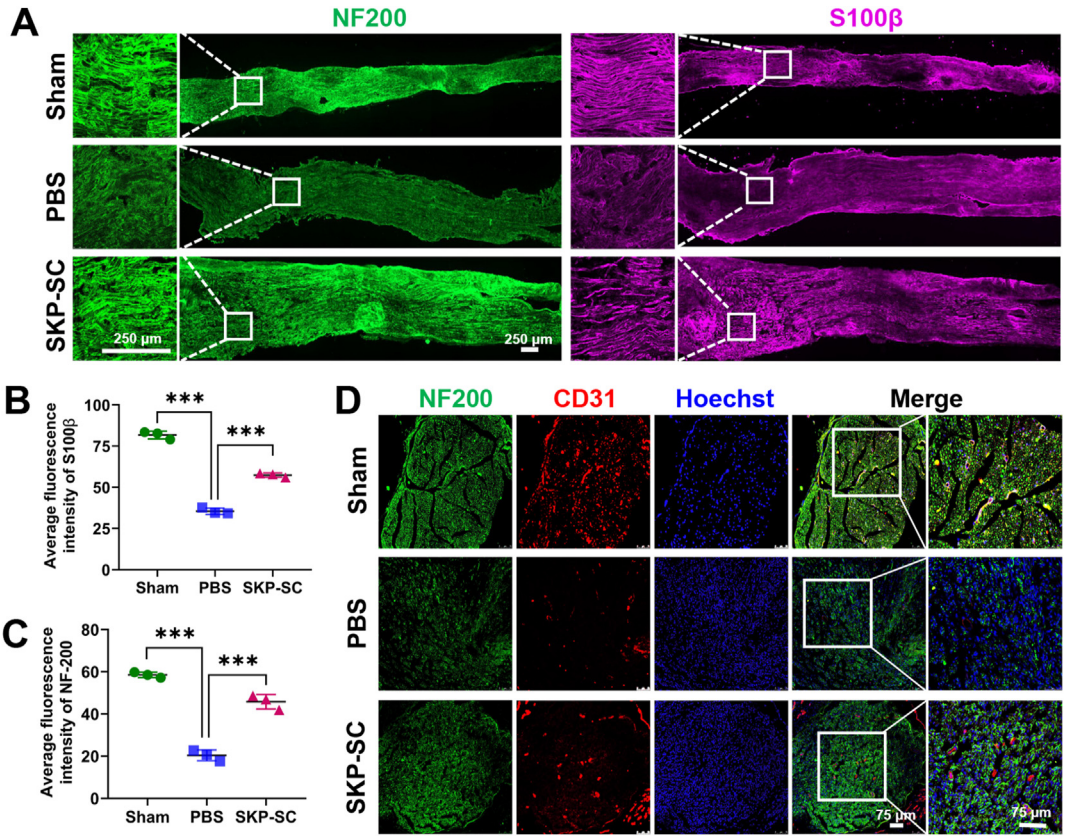

Fig. 3. The pro-regenerative effect of SKP-SCs on injured branchial plexus. (A) Representative image of nerve regeneration in three groups in vivo. NF200 (green) stained regenerating neurofilaments and S100β (purple) stained Schwann cells showed the higher fluorescence intensity expressed in SKP-SC group than that in PBS group. Scale bar, 250 μm. (B, C) Statistical histograms showed the average fluorescence intensity of NF200 and S100β of regenerated nerves among three groups. Data are presented as Mean ± SEM, $n = 3$; *, $p < 0.05$; **, $p < 0.01$; ***, $p < 0.001$. (D) The regeneration of neurovascular bundles in three groups in vivo showed the expression CD31 (red) in three groups, with NF200 (green) labeled neurofilaments and Hoechst (blue) labeled nucleus. Scale bar, 75 μm.

sections, and the average cross-sectional area of muscle fibers was consistent with Masson's trichrome staining muscle fibers in each group statistically (Fig. 6A and B).

Third, longitudinal frozen muscle sections displayed that most of the motor endplates in PBS group were immature plaque compared with mature pretzel ones in sham group, while there were more mature and intermediate motor endplates in SKP-SC group compared with that in PBS group (Fig. 6C). That suggested the neuromuscular junction remodeling.

3.6. SKP-SC-CM treatment improved cell viability and neurites growth of MNs

After culture for 4 days, MNs showed axonal outgrowth with sprouting branches and bright cell bodies (Fig. 7A). Immunofluorescence staining indicated that MNs positively co-expressed ChAT and TUJ1, and the purity was more than 95%, that suggested the cultured MNs can be used for subsequent experiments (Fig. 7B).

To investigate whether SKP-SC-CM can promote the recovery of the cell viability and neurite growth of injured MNs, we established a neuron OGD injury model as above. CCK8 test found that the cell viability of motor neurons decreased to about 60% in OGD group compared to the control group, while increased significantly in SKP-SC-CM treatment groups with different concentrations in a dose-dependent manner. When the concentration reached 10%, the cell viability was similar to the control group. It's more obvious that the cell viability has exceeded that of the control group when the concentration reaches 20%. Collectively, SKP-SC-CM can repair the cell viability of OGD-injured neurons significantly (Fig. 7C).

Immunostaining experiment was performed to evaluate the MNs growth discovered that OGD could cause neuronal cell death and axonal rupture, besides that the neurite length was significantly shorter and the number of branches was significantly reduced compared with the control group. After treatment with 20% SKP-SC-CM, the phenomenon of axonal rupture alleviated significantly (Fig. 7D). This was further illustrated by the average length of the longest neurites and the average branch numbers of neurites (Fig. 7E and F). The results demonstrated that neuronal morphology in OGD group was significantly impaired than that in the control group, while compared with OGD group, that was ameliorated significantly in SKP-SC-CM group.

3.7. Bioinformation analysis of SKP-SC-CM contained cytokines

First, the mean signal values of the detected 67 cytokines varied from 505 to 2784 relatively, among them 36 SKP-SC-sourced cytokines with greater expression abundance (Mean signal values more than 1000) have been screened out. After retrieval, analysis, and summary of the annotation information provided for *Rattus norvegicus* by UniProt database, finally 32 informative cytokines were deemed to be relevant to neural regenerative process. The histograms showed the involved cell type number (upper panel) (Fig. 8) of 32 candidate cytokines (bottom panel) respectively. The GO clusters of these cytokines involved in different cellular biological processes of distinct cell types were presented in scatter plot (middle panel) (Fig. 8).

Moreover, the implicated cytokine number of each biological process of each cell type, involving with neurons, Schwann cells,

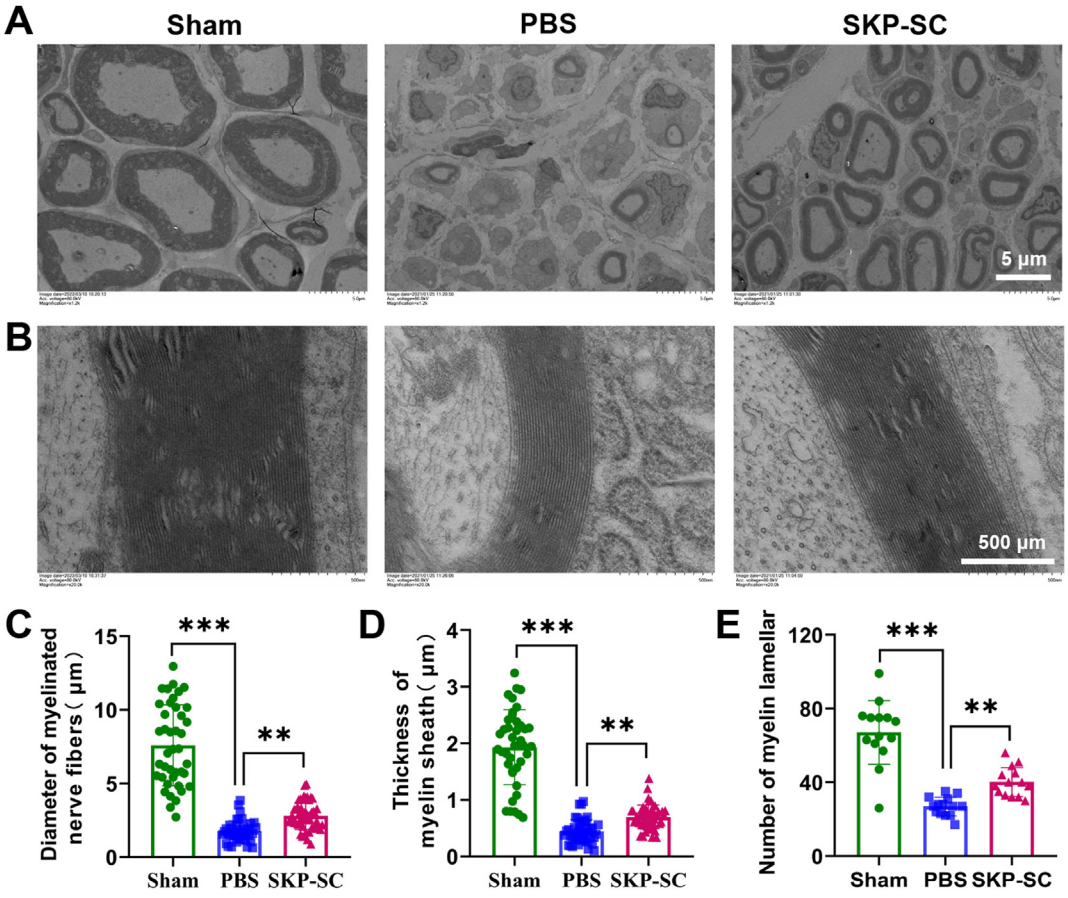

Fig. 4. The evaluation of the ultrastructure of the regenerated nerve fibers under transmission electron microscope. (A) Representative images of the regenerated nerve fibers (Scale bar, 5 μm) and (B) the myelin lamellar in three groups (Scale bar, 500 nm). Statistical analysis of (C) the diameter of myelinated nerve fibers ($n > 40$), (D) the thickness of myelin sheath ($n > 40$), and (E) the number of myelin lamellar ($n = 14$) of the regenerated nerve fibers in three groups. Data are presented as Mean ± SEM. **, $p < 0.01$; ***, $p < 0.001$.

inflammatory cells, vascular endothelial cells, and SKP-SCs, were displayed in corresponding histograms (right panel), matched to MESH terms (left panel) respectively (Fig. 8). For neurons, mainly there were 21 cytokines associated with 4 relevant biological processes, including apoptosis inhibition (17), neurogenesis (10), axon extension (5), and axon guidance (3). For Schwann cells (SCs), mainly there were 24 cytokines involved with cell proliferation (19), cell migration (16), apoptosis inhibition (14), and cell adhesion (10) respectively, 4 clusters were enriched. For VECs, mainly there were 26 cytokines relevant to 5 clusters respectively, including cells proliferation (20), cell migration (17), apoptosis inhibition (15), angiogenesis (11), and cell adhesion (10). For inflammatory cells, mainly there were 24 cytokines implicated with cell chemotaxis (15), inflammation regulation (12), cell proliferation (9), and cell differentiation (7) respectively, 4 clusters were enriched. Concerned to the implanted SKP-SCs themselves, there were 21 main cytokines related with 4 cell responsive clusters, respectively to inflammation (14), to hypoxia (9), cell metabolism (9, including cell response to ATP, glucose and insulin), and to growth factors (4) (Fig. 8).

3.8. Expression of the hypoxia responsive cytokines at mRNA level in SKP-SCs

In order to screen the key cytokines that exerting vital effects on nerve injury microenvironment regulation, we performed RT-PCR detection of nine hypoxia responsive cytokines in hypoxia-treated SKP-SCs compared to normoxia SKP-SCs. The results showed that at 24 h after hypoxia, the mRNA expression of platelet-derived growth factor-AA (PDGF-AA), vascular endothelial growth factor-A (VEGF-A) and interleukin-1 beta (IL-1β) in SKP-SCs were significantly elevated, other cytokines did not show marked increase in hypoxia SKP-SCs than that in normoxia SKP-SCs (Fig. 9).

4. Discussion

Adult traumatic BPI are occurring with growing frequency, the devastating outcome that even be life-altering seems require a multidisciplinary team approaches to address [34,35]. To explore novel medical approaches, the present work investigated the repair effect of combining local SKP-SCs implantation with end-to-end neurorrhaphy on BPI post-neurotomy. In developmental studies, SKP-SCs originate from neural crest cells, the ancestor of the Schwann cells. Here rat SKP-SCs implantation were proved enable to enhance the therapy efficacy and reached morphology and function reconstruction after rat LBPI, in accordance with previous work on sciatic nerve injury [36]. Besides, SKP-SC-CM displayed repair effect on cell survival and neurite regrowth of OGD-injured MNs in vitro, that attracted our focus on secretome. Additionally, GO annotations of cytokines detected in SKP-SC-CM were sorted out through manual cluster enrichment analysis based on UniProt database. We take the 32 cytokines as example, provided recognition on how SKP-SCs affects various biological processes of diverse types of cells in paracrine soluble molecular level, and speculated the possible key reverberations of SKP-SC-secretome on multiple cell types for creating neural regenerative microenvironment.

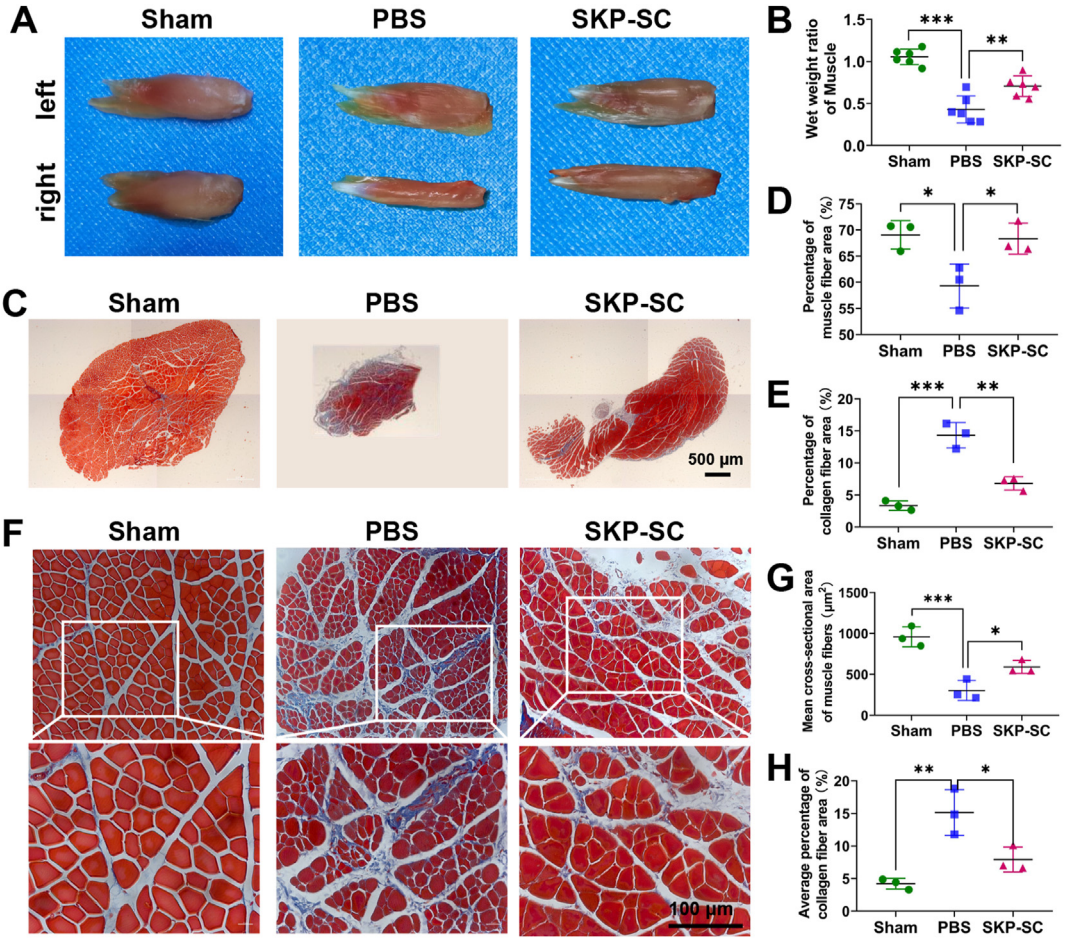

Fig. 5. Analysis of the gross morphology and Masson's trichrome staining of target muscles paraffin section. (A) Representative gross photograph of bilateral biceps muscles of three groups at six weeks postoperatively. (B) Histograms showed the wet weight ratios of targeted muscles (right injured side/left contralateral uninjured side) in three groups ($n = 6$). (C) Representative overall images of Masson's trichrome staining biceps muscles paraffin sections in three groups (Scale bar, 500 μm). Statistical histograms showed (D) the percentage of muscle fiber area and (E) the collagen fiber area in the whole muscle ($n = 3$; 3 fields per rat). (F) Representative images of regional biceps muscles paraffin sections in three groups (Scale bar, 100 μm). (G) Statistical histograms showed the mean cross-sectional area of muscle fibers and (H) the average percentage of collagen fiber area in the regional muscle ($n = 3$; not less than 4 random fields per rat). Data are presented as Mean ± SEM. *, $p < 0.05$; **, $p < 0.01$; ***, $p < 0.001$.

Firstly, during the process of branchial plexus anatomy and injury model construction in SD rats, we found that it was less infeasible to remove the clavicle and more muscles to expose truncus superior of branchial plexus, because that could lead to unreasonable harm to the animals, owning to the location of C5 and C6 of branchial plexus in SD rats was too deeper compared to that in Wistar rat s [33,37,38]. Depending on that, here SD rats were proved proper to establish the infraclavicular types of traumatic BPI model with applied traction and transection, as that, lower brachial plexus injury (LBPI) was established in this study.

In this work, taking the advantage of SKP-SCs with proliferating capacity and multiple passaging stability, in vitro expanded SKP-SCs were sufficient for implantation to treat rat traumatic LBPI, then the repair effects were ascertained through behavioral function evaluation and tissue morphology assessment. The results of TGT evaluating the restoration of elbow flexion and shoulder stability, and cold sensitivity test evaluating pain sense recovery, showed significantly enhanced recovery of rat forelimb locomotive and sensory function, in agreement with electrophysiological examination recording CMAP improvement. Furthermore, the therapeutic effects of SKP-SCs were demonstrated through the vascular regeneration companied with the nerve regrowth, and the axonal remyelination with thicker clear lamellar sheath morphology. Moreover, morphometric analysis of reinnervated muscle indicated that implanted SKP-SCs might dramatically attenuate target muscle atrophy, augment motor endplate remodeling, highlighting the improved support and nourishment efficacy of regenerative brachial plexus on muscles. Previously researchers found the synergistic role of allogenic SKP-SCs and acellular nerve allograft on nerve regeneration [39], similarly, recently researchers developed a tissue engineered nerve graft modified with extracellular matrix generated by SKP-SCs and expanded its application in defect of upper BPI [40]. While this work proved the repair effect of SKP-SCs on LBPI. These findings evidenced that SKP-SC-based therapy can markedly promote the recovery of traumatic PNI, in agreement with the reported review regarding the role of Schwann cell-sourced secretome [18].

Additionally, the underlying mechanisms of the repair effects of implanted SKP-SCs on PNI were paracrine secretome dependent, that was further implied in this work. Since it was reported that, the transection of peripheral nerves in rodents may retrogradely induce death of parent MNs in the spinal cord, and motor axon degeneration, and de-innervation of targeted muscles, resulting in serious functional deficits in the forelimb [9]. Therefore, here the sequent damage of MNs was simulated in vitro and treated with SKP-SCs-sourced secretome, which really could alleviate cellular

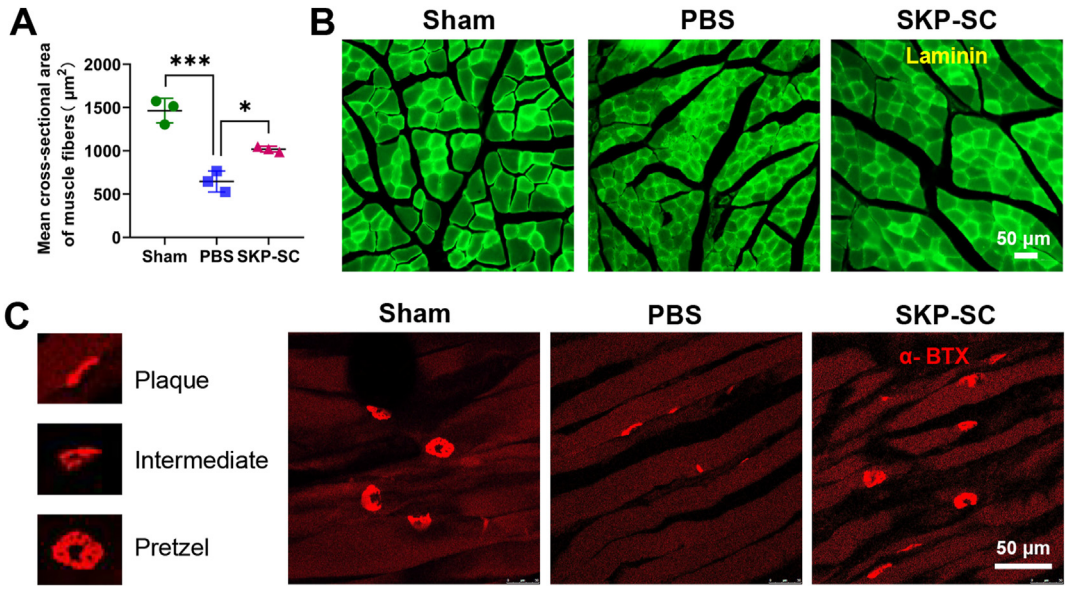

Fig. 6. Cross-sectional area of muscle fibers and neuro-muscular junction analysis of target muscles freezing section. (A) Statistical histograms showed the average cross-sectional area of targeted muscle fibers ($n = 3$; not less than 9 random fields per rat). (B) Representative images of laminin immunostaining of cross-section of targeted muscles in different groups. (C) Representative images of α-bungarotoxin staining of motor endplates in three groups, showing mature pretzel, intermediate morphology, or immature plaque. Data are presented as Mean ± SEM. *, $p < 0.05$; ***, $p < 0.001$. Scale bar, 50 μm.

death and neurite rupture of OGD-injured MNs. Moreover, the interaction between endogenous Schwann cells and other cells during repair of PNI has been highlighted [41], thus it was essential that the exogenous SKP-SCs might interact with distinct types of cells post-implantation via secretome signals. Given that, further confirmation on what cytokines derived from implanted exogenous SKP-SCs communicated with various endogenous cell types via paracrine secretome arising our interest.

As crucial players in the progression or regression of a pathological process, these molecules provide a window through which mechanisms can be explored. The Sensitivity and repeatability advantage of protein chip array was utilized in this work. In order to measure cytokine levels, an array assay of 67 rat cytokines was performed, next, the associated 32 cytokines with greater detecting value in SKP-SC-CM were classified depending on the annotated biological functions, and matched with the function-related cell types in a scatter-plot manner. The cluster enrichment analyses findings of shared or unique or superimposed cytokines ensembles information further demonstrated that various cellular biological processes of Schwann cells, VECs and inflammatory cells could be effectively coordinated by exogenous SKP-SCs-sourced secretome components.

First and foremost, the bioinformatic analysis results indicated that transplanted SKP-SCs perhaps maintained own cellular metabolism for survival via response to ATP, glucose, insulin and growth factors in microenvironment, through autocrine of corresponding cytokines. There are 11 associated cytokines were enriched according to annotations. It was demonstrated that a variety of classic biologic molecules and mediators are beneficial to creating permissive microenvironment for cell implantation [42]. Up to date, IL-4 has been identified as a promising signaling pathway target for traumatic PNI repair, the IL-4 responding cells implicated in nerve regeneration including Schwann cells, macrophages, fibroblasts, and neurons, which either indirectly via other immune cells, or promoting nerve regrowth directly [43].

Notably, the response of SKP-SCs to hypoxic microenvironment could induce the relevant cytokines secretion, here defined as a panel of hypoxia-responsive cytokines (HRCK). Intriguingly, each HRCK as signal target may initiate diverse biological process regulation of implicated endogenous cell types in neural microenvironment. For instance, Fractalkine (namely chemokine (C-X3-C motif) ligand 1, CX3CL1) was identified as a signal inducing microglia-mediated synapse elimination to regulate synaptic connectivity [44] and mitigating inflammation [45]; Intercellular adhesion molecule-1 (ICAM-1) was reported could protect neurons against Amyloid-β and improve cognitive behaviors in mice by inhibiting NF-κB [46]; Monocyte chemoattractant protein-1 alpha (MCP-1α, namely chemokine (C–C motif) ligand 2, CCL2) has been identified involved in the autophagy and apoptosis signaling pathway axis after spinal cord injury [47]; Notch1 signaling pathway has been reported could promote angiogenesis of cerebral microvasculature to protect ischemia reperfusion injury [48]; Soluble tumor necrosis factor-alpha (TNF-α) selectively inhibition was reported could change the neuroinflammatory response after moderate spinal cord injury in mice [49]; Interleukin-1 alpha (IL-1α) preconditioned mesenchymal stem cells exhibited promotive neuroprotection properties for ischemic stroke mice [50]; while IL-1β was reported as inhibitory target in inflammsome axis-mediated neutrophil infiltration could protect neurons in neurodegenerative disease [51]; PDGF-AA has been reported could improve the function recovery of spinal cord injury via subcutaneous administration [52]; and VEGF-A has been reviewed as the leading promoter of angiogenesis in health and disease, thus became the therapeutic targeting [53]. Therefore, the possible modulation effect of HRCK on neuronal and non-neuronal cells in neural injury position was especially concerned in our multiple cluster analyses.

Meanwhile, the implanted SKP-SCs also might directly response to inflammation micro-circumstance and then release associated cytokines, that comprise the HRCK except for Notch 1 and PDGF-AA, added other 7 factors. Taken together, above-mentioned total 21 cytokines involved in SKP-SCs response to extracellular stimulation possibly could facilitate the exogenous SKP-SCs to adapting to the acute inflammation microenvironment after implantation post-nerve-injury, and speeding the clearance process of demyelinated debris of Wallerian degeneration. Thus, inflammatory regulation is indispensable in acute neuroinflammatory phase [54], SKP-SCs

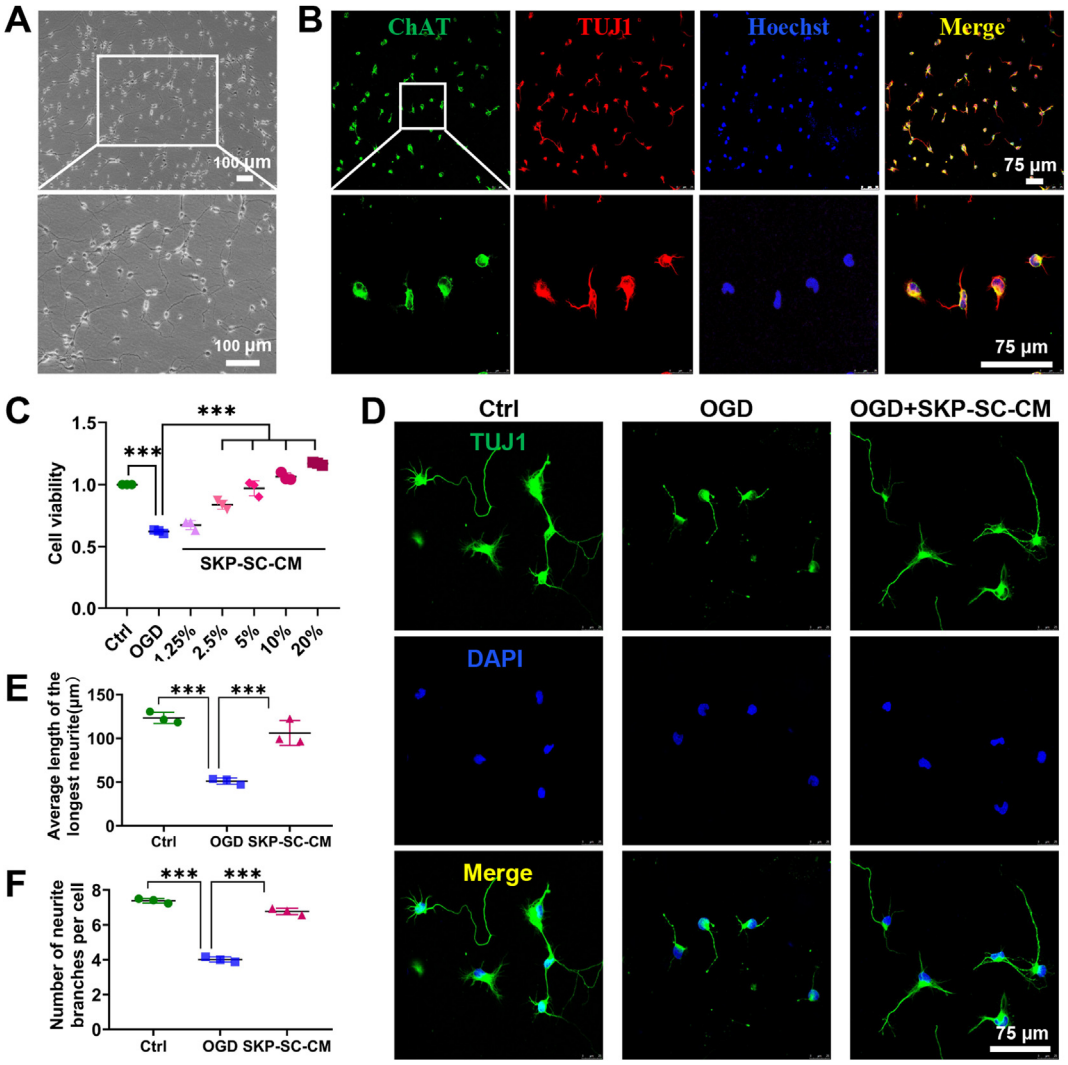

Fig. 7. Identification of motor neurons and treatment of OGD-injured neurons with SKP-SC sourced conditioned medium (SKP-SC-CM). (A) Morphology of primarily cultured motor neurons with extended neurites forming a network at day 4. Scale bar, 100 μm. (B) Immunofluorescence stained motor neurons positively expressed ChAT (green) and TUJ1 (red) with Hoechst labeled nuclei (blue). Scale bar, 75 μm. (C) Statistical histograms showed the increasing neuronal cell viability in a dose-dependent manner. (D) Immunofluorescence stained motor neurons positively expressed TUJ1 (green) in each group (control, OGD, OGD + SKP-SC-CM). Scale bar, 75 μm. (E, F) Statistical histograms of the average longest neurite length and the number of primary neurites per cell was better in OGD + SKP-SC-CM group than that in OGD group. For each group and experiment, about 100 neurons per condition were assessed. Data are presented as Mean ± SEM, n = 3; ***, $p < 0.001$.

implantation might potentiate to recruit various type of inflammatory cells to injurious plot by respective cytokines.

As well known, white blood cell exudation is the most important feature of the inflammatory response, which contain a variety of inflammatory cells. Here total 15 cytokines are contained relevant to inflammation cell chemotaxis, among them 12 factors overlapping with above sorted SKP-SCs inflammation response cytokines cluster. Besides, plus 3 cytokines: Galectin-3 relative to neutrophils, eosinophils, and monocyte-macrophages, even lymphocytes chemotaxis; triggering receptor expressed on myeloid cells 1 (TREM-1) relate to neutrophils and macrophages chemotaxis; particularly VEGF-A annotated relation to mast cell chemotaxis. Recent decade, the recruitment of inflammatory cells has been growingly reported, especially, macrophages are the most notable cell type, showing active phenotype polarization and recuperative potency for axonal regeneration [55,56].

In order to sustain controllable inflammation regulation, cell proliferation of lymphocytes might be induced in vivo. IL-2 and IL-4 was annotated relative to both T cell and B cell proliferation. Particularly, Galectin-3, gp130, interferon gamma (IFN-γ), IL-1α, IL-1β, IL-13 was annotated relevant to T cell proliferation. Although fibroblast cells proliferation also probably participates into the inflammatory process triggered by PDGF-AA, simultaneously IFN-γ might exert negative regulation of fibroblast proliferation. Moreover, self-renewing macrophages in dorsal root ganglia has been reported contribute to promote nerve regeneration [57].

Inflammation cell differentiation also involved in the inflammatory regulation process, the analyzed clustering results showed there are 7 cytokine factors related to the differentiation process of distinct inflammatory cell types respectively. For instance, IL-1 R6, IL-2 [58], IL-4, in positive regulation of T cell differentiation; IL-4 in dendritic cell and T-helper 2 cell differentiation; and VEGF-A relate to monocyte and macrophage differentiation. As far novel tissue macrophage subsets have already been revealed in work performed within large international projects, such as the Human Cell Atlas, because in inflammatory conditions, myeloid cells exhibit substantially vaster heterogeneity than previously anticipated [59].

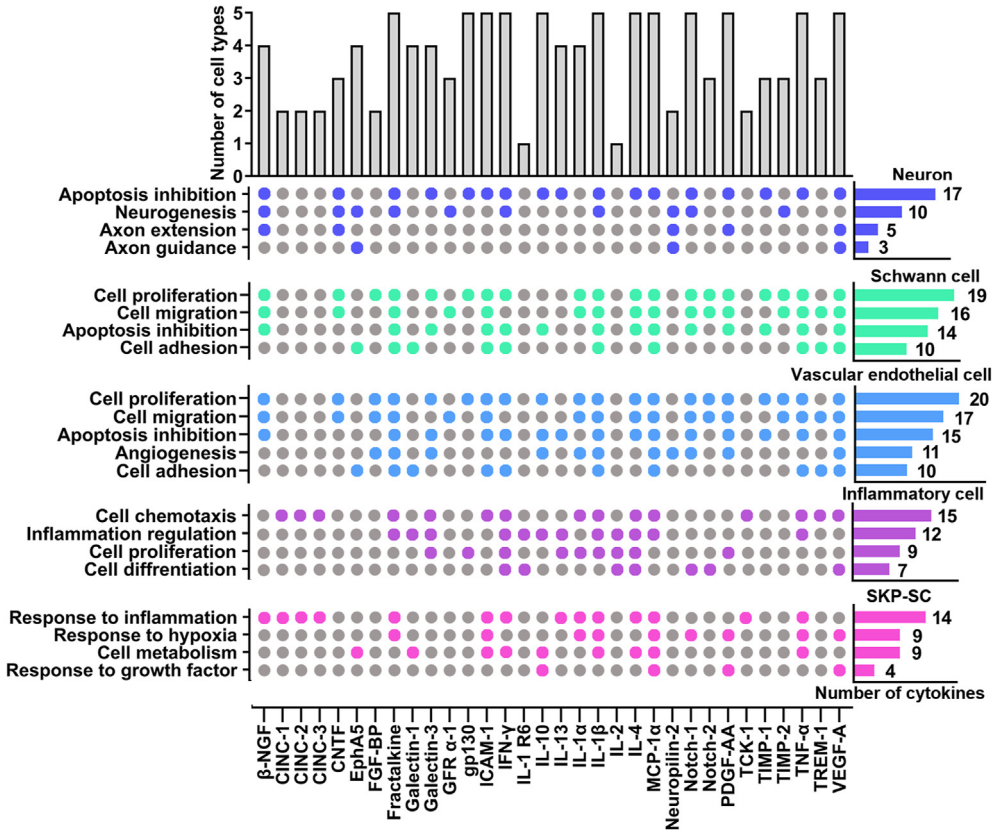

Fig. 8. Bioinformatic cluster analysis and classification of screened cytokines contained in SKP-SC-CM. (Upper panel) The histograms showed the involved cell type number of (Bottom panel) 32 informative cytokines respectively. (Middle panel) The different candidate cytokines involved in 5 cell types, associated cellular biological processes were presented in the scatter plots. (Right panel) the implicated cytokine number of each cellular biological process, involving with neurons, Schwann cells, inflammatory cells, VECs, and implanted SKP-SCs, were displayed in histograms, corresponding to biological process terms (Left panel) respectively.

Certainly, inflammation regulation as the key biological process involved in SKP-SC-secretome triggering in microenvironment, beyond the chemotaxis, proliferation and differentiation modulation, because the balance modulation between anti-inflammation and pro-inflammation is vital to remain the neural microenvironment homeostasis [60]. Although Galectin-1 and above-mentioned so many cytokines can join in positive regulation of inflammation, IL-2, IL-4, IL-10, together with IL-13 can exert negative regulation of inflammatory response. Besides, Fractalkine might negatively regulate the IL-1α production, TNF production, and microglial cell activation. Since inflaming impairs peripheral nerve homeostasis maintenance and regeneration [61], manageable inflammation is beneficial to anti-impairment and anti-apoptosis, excessive or persistent inflammation would incite further tissue destruction.

Besides, both in peripheral nerve degeneration and regeneration process, apoptosis inhibition is critical to not only neurons, also Schwann cells and VECs. These cells are indispensable to neuronal growth milieu homeostasis reconstructing. In our findings, SKP-SC-CM provided abundant cytokines to suppress apoptosis. Among the screened cytokines, HRCK participate in neuronal apoptosis inhibition, despite IL-1α not be cited as apoptosis inhibitor, 6 more cytokines, including β-NGF, galectin-3, IFN-γ, IL-4, IL-10, tissue inhibitors of metalloproteinase-1 (TIMP-1), cited as apoptosis suppressors. Moreover, the inhibitory action of IL-13 on VECs and neurons apoptosis has been cited into database, as well as the apoptosis inhibition activity of ciliary neurotrophic factor (CNTF) and gp130 on neurons has been quoted. Notably, the first selective inhibitor of IL-6 trans-signaling, gp130, has shown therapeutic potential in various preclinical models of disease [62]. The cluster enrichment analyses results suggested that SKP-SC promise to enhance the survival of damaged neuronal cells, Schwann cells, and VECs via secretome exerting anti-apoptosis activity [18].

Overriding the acute neuroinflammation phase, Schwann cells [63,64] and VECs [65] are both subject to cell proliferation and migration process. Simultaneously, results enumerated abundant cytokines for promoting the proliferation of Schwann cells and VECs, based on apoptosis inhibition cytokines for Schwann cells and VECs, 6 more cytokines can present positive regulation of cell population proliferation, some of them (CNTF, IL-1α, Notch-2 and TIMP-2) can modulate MAPK pathway or ERK1/ERK2 pathway, which is well known responsible to cell survival and growth. Specially, IL-10 is only quoted responsible to VECs proliferation. Furthermore, cell migration related cytokines are also essential for the activation of Schwann cells [66] and VECs, HRCK are incorporated within this cluster, and 8 more cytokines are listed out. Among them, β-NGF is positive regulator of ERK1/ERK2 cascade for migration activation, specially, fibroblast growth factor-binding protein (FGF-BP) is only cited responsive to positive regulation of VECs migration, that involved in sprouting angiogenesis of VECs.

Moreover, cell adhesion associated cytokines were clustered for Schwann cells and VECs, based on 6 cytokines from HRCK, 4 more cytokines are highlighted on, including erythropoietin-producing hepatocyte A5 (EphA5), Galectin-1, IFN-γ, and TREM-1. It was reported that, Fractalkine could upregulate IACM-1 expression in endothelial cells through CX3CR1 and promote neutrophil adhesion via the Jak-Stat5 pathway [67]. Recently reported, repair

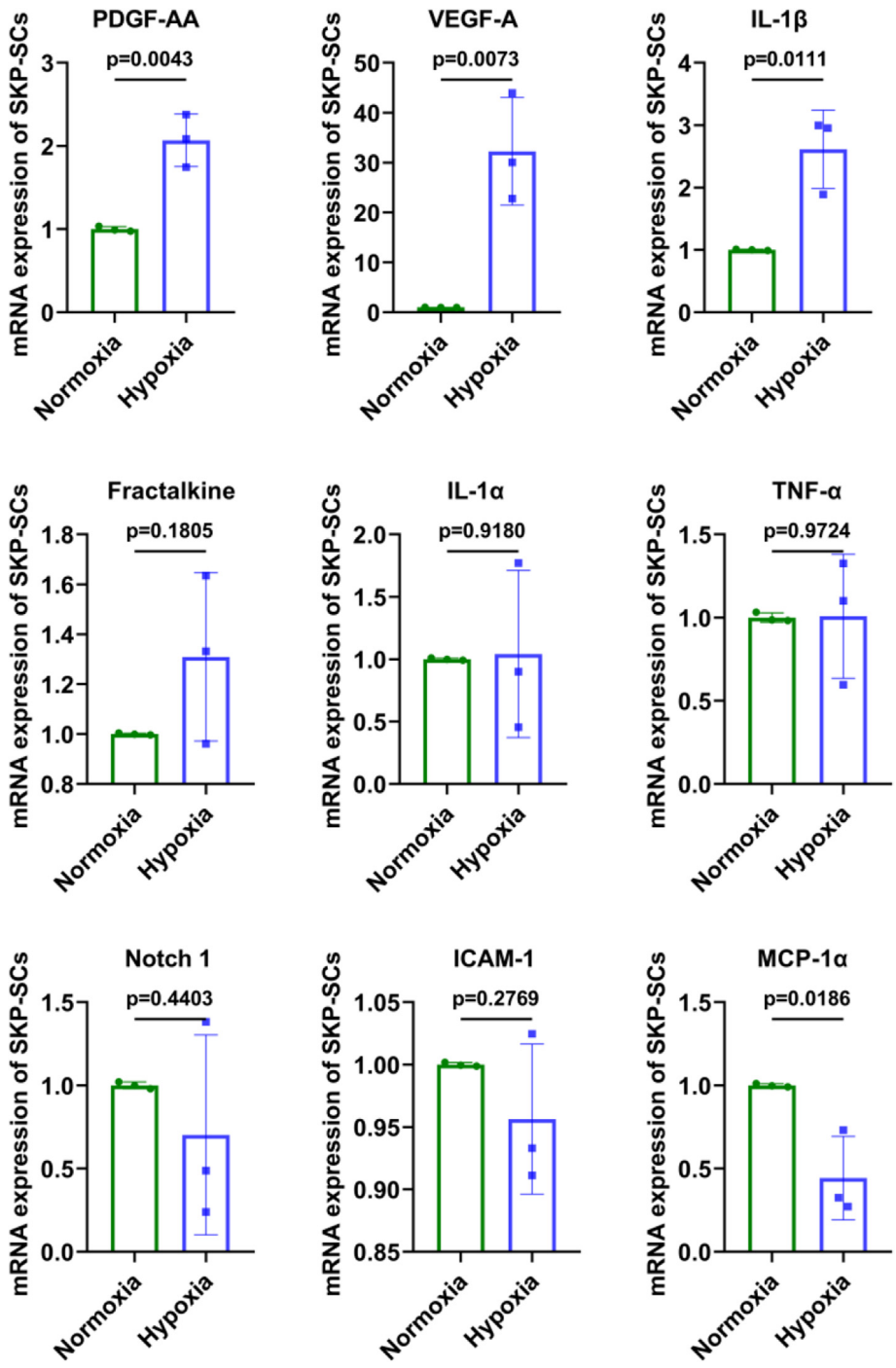

Fig. 9. Expression of the hypoxia responsive cytokines at mRNA level in SKP-SCs. The histograms showed that at 24 h after hypoxia, the mRNA expression of PDGF-AA, VEGF-A and IL-1β in SKP-SCs were significantly elevated, other cytokines did not show marked increase in hypoxia SKP-SCs than that in normoxia SKP-SCs.

phenotype Schwann cell might have greater adherent properties with more cellular processes than non-repair phenotype Schwann cells [68].

Furthermore, angiogenesis is a characteristic and essential process involved in peripheral nerve regenerative processes [65], the initiation of VECs via SKP-SCs secretome is worth to be analyzed. Then the associated 11 factors were itemized together, based on HRCK (except for ICAM-1 and TNF-α), 4 more cytokines are FGF-BP, Galectin-3, IL-10, and Neuropilin-2, providing pro-angiogenic cues to VECs. FGFBP1 signaling axis plays an important role in the regulation of angiogenesis in VECs that reported as a potential therapeutic target for anti-angiogenic therapeutics [69]. Recently angiogenesis was reported can be promoted to protect neural tissue via activating HIF-1alpha-VEGFA-Notch1 signaling pathway [48]. Patho-physiologically, cytokines produced by SKP-SCs might together with cues of nerve injury promote the vascular network shaping, then the vascular niche can create a permissive environment that enables different cell types to realize

their regenerative program [70], not limited to providing blood and oxygen via vessels. Particularly, the tubule structure of neovascularization might serve as scaffold bridge for Schwann cells to migrate between two stumps of nerve gap [71], recently SKP-SCs was reported can be applied to enhance repair complete nerve transection via efficiently constructing pre-vascularized tissue-engineered peripheral nerves [72].

Finally, comparing angiogenesis with neurogenesis, there existed substantial difference between two biological process, but they shared factors such as Fractalkine [73], IL-1β [74], Neuropilin-2 [75], and Notch1 [76] that closely relate to the neural development and regeneration process regulation. Similarly, a pro-angiogenic potential of the secretome from human skin-derived multipotent stromal cells on wound healing has been verified through an endothelial cell tube formation assay [77]. The 4 shared factors together with other 6 more cytokines are clustered closely relative to neurogenesis process, indicating the possible to evoke neural regeneration. Among the above-listed 10 cytokines relevant to neurogenesis, 3 cytokines (EphA5, Neuropilin-2 and VEGF-A) regarding to axon guidance, and 4 cytokines (β-NGF, CNTF, Neuropilin-2 and VEGF-A) regarding to axon extension, are laid out respectively. In addition, PDGF-AA has been highlighted in relation to axon guidance, it was reported related with retinal ganglion cell neuroprotection [78].

However, it required to be considered that the bioinformatic analysis of rat cytokines is not equal to other species such as mice and human, also limited by the refreshing speed of database version. In this study, we attempted to provide a paradigm towards recapitulating the microenvironment response to exogenous SKP-SCs via secretome, and analyzing the possible effector molecules and mechanisms of SKP-SC-based therapy in the insight of microenvironment improvement. Additionally, we further narrowed down 9 HRCK to 3 cytokines, PDGF-AA, VEGF-A and IL-1β, according to the elevated mRNA expression level in hypoxia-treated SKP-SCs. Particularly, PDGF-AA and VEGF-A highly secreted from SKP-SCs responsive to hypoxia involved in both the neuronal and non-neuronal biological processes above-mentioned. The novel molecular response and downstream signaling pathways of implicated kinds of cell types to SKP-SCs secretome components remain to be further verified via overexpression and inhibitory experiments. Notably, to further engineer the secretome, tailor its therapeutic effects and the delivery strategies [79], define the SKP-SC secretome in an inflammatory, hypoxic, and oxidative stress microenvironment simulating post-implantation might be a challenged work in future, further trials in vivo for pro-neuroregeneration are also essential, that would provide solid underpinnings to cell-free therapy, including precise molecule-therapy [43] and gene-therapy [80]. The present work anticipated application prospect of SKP-SCs-based therapy for neural repair and regeneration.

5. Conclusion

Collectively, this study provided therapeutic efficacy of combining neurorrhaphy with cell implantation for traumatic LBPI repair and repair effect of SKP-SC-secretome on damaged MNs. Here we cluster enriched 32 cytokines from SKP-SC-secretome and especially concerned on cytokines responded to hypoxia, termed as HRCK, that were annotated associating with distinct cell types and various biological process corresponding to nerve regeneration, especially focused on PDGF-AA and VEGF-A. It was demonstrated that SKP-SCs can create a permissive milieu homeostasis for neuronal survival and axonal regeneration. In further work, the SKP-SC-secretome not limited in HRCK would provide more targets for promoting the translational prospect for cell-based therapy application strategy.

Data availability statement

The data that supporting the findings in this study are available from the corresponding author upon reasonable request.

Author contributions

Conceptualization, H.S. and J.C.; Data curation, J.C., X.Y., and H.S.; Formal analysis, X.Y., J.C., H.S, M.C. and. L.Z.; Funding acquisition, H.S., M.C., and H.X.; Investigation, H.X., H.S., Y.Y., Q.H. and J.C.; Methodology, X.Y., J. C., M.C., X.W. and L.W.; Project administration, H.S.; Supervision, F.D. and H.S.; Validation, X.Y., J.C., X.W., L.W. and L.S.; Writing—original draft preparation, J.C. and X.Y.; Writing—review and editing, H.S.; All authors have read and agreed to the published version of the manuscript.

Declaration of competing interest

The authors declare no conflict of interest.

Acknowledgments

This work was supported by the Jiangsu Province Science and Technology Plan Project (Youth Fund Project) [No. BK20230607], the Basic Science (Natural Science) Research General Project of Jiangsu Province Higher Education Institutions (No. 23KJB180022), the Jiangsu Funding Program for Excellent Postdoctoral Talent (2022), the National Natural Science Foundation of China (No. 31870977), Nantong Science and Technology Bureau (Social and livelihood of Public health Program) (No. MS12021007), and Priority Academic Program Development of Jiangsu Higher Education Institutions [PAPD].

References

[1] Kaiser R, Waldauf P, Ullas G, Krajcova A. Epidemiology, etiology, and types of severe adult brachial plexus injuries requiring surgical repair: systematic review and meta-analysis. Neurosurg Rev 2020;43:443–52.
[2] Pejkova S, Filipce V, Peev I, Nikolovska B, Jovanoski T, Georgieva G, et al. Brachial plexus injuries - review of the anatomy and the treatment options. Prilozi 2021;42:91–103.
[3] Dixit NN, McCormick CM, Warren E, Cole JH, Saul KR. Preganglionic and postganglionic brachial plexus birth injury effects on shoulder muscle growth. J Hand Surg 2021;46:146 e1–e9.
[4] Doshi RM, Reid MY, Dixit NN, Fawcett EB, Cole JH, Saul KR. Location of brachial plexus birth injury affects functional outcomes in a rat model. J Orthop Res : official publication of the Orthopaedic Research Society 2022;40:1281–92.
[5] Lauretti L, Pallini R, Romani R, Di Rocco F, Ciampini A, Gangitano C, et al. Lower trunk of brachial plexus injury in the neonate rat: effects of timing repair. Neurol Res 2009;31:518–27.
[6] Xu QG, Forden J, Walsh SK, Gordon T, Midha R. Motoneuron survival after chronic and sequential peripheral nerve injuries in the rat. J Neurosurg 2010;112:890–9.
[7] Vu AT, Sparkman DM, van Belle CJ, Yakuboff KP, Schwentker AR. Retropharyngeal contralateral C7 nerve transfer to the lower trunk for brachial plexus birth injury: technique and results. J Hand Surg 2018;43:417–24.
[8] Zhang M, Li C, Liu SY, Zhang FS, Zhang PX. An electroencephalography-based human-machine interface combined with contralateral C7 transfer in the treatment of brachial plexus injury. Neural regeneration research 2022;17:2600–5.
[9] Binder MD, Powers RK, Heckman CJ. Nonlinear input-output functions of motoneurons. Physiology 2020;35:31–9.
[10] Martinez-Gonzalez L, Martinez A. Emerging clinical investigational drugs for the treatment of amyotrophic lateral sclerosis. Expet Opin Invest Drugs 2023;32:141–60.
[11] Nicoletti VG, Pajer K, Calcagno D, Pajenda G, Nogradi A. The role of metals in the neuroregenerative action of BDNF, GDNF, NGF and other neurotrophic factors. Biomolecules 2022;12.
[12] Spejo AB, Carvalho JL, Goes AM, Oliveira AL. Neuroprotective effects of mesenchymal stem cells on spinal motoneurons following ventral root axotomy: synapse stability and axonal regeneration. Neuroscience 2013;250:715–32.

[13] Su H, Wang L, Cai J, Yuan Q, Yang X, Yao X, et al. Transplanted motoneurons derived from human induced pluripotent stem cells form functional connections with target muscle. Stem Cell Res 2013;11:529–39.
[14] Pajer K, Bellak T, Nogradi A. Stem cell secretome for spinal cord repair: is it more than just a random baseline set of factors? Cells 2021;10.
[15] Pajer K, Feichtinger GA, Marton G, Sabitzer S, Klein D, Redl H, et al. Cytokine signaling by grafted neuroectodermal stem cells rescues motoneurons destined to die. Exp Neurol 2014;261:180–9.
[16] Giovannelli L, Bari E, Jommi C, Tartara F, Armocida D, Garbossa D, et al. Mesenchymal stem cell secretome and extracellular vesicles for neurodegenerative diseases: risk-benefit profile and next steps for the market access. Bioact Mater 2023;29:16–35.
[17] Pearse DD, Bastidas J, Izabel SS, Ghosh M. Schwann cell transplantation subdues the pro-inflammatory innate immune cell response after spinal cord injury. Int J Mol Sci 2018;19.
[18] Contreras E, Bolivar S, Navarro X, Udina E. New insights into peripheral nerve regeneration: the role of secretomes. Exp Neurol 2022;354:114069.
[19] Gersey ZC, Burks SS, Anderson KD, Dididze M, Khan A, Dietrich WD, et al. First human experience with autologous Schwann cells to supplement sciatic nerve repair: report of 2 cases with long-term follow-up. Neurosurg Focus 2017;42:E2.
[20] Biernaskie JA, McKenzie IA, Toma JG, Miller FD. Isolation of skin-derived precursors (SKPs) and differentiation and enrichment of their Schwann cell progeny. Nat Protoc 2006;1:2803–12.
[21] McKenzie IA, Biernaskie J, Toma JG, Midha R, Miller FD. Skin-derived precursors generate myelinating Schwann cells for the injured and dysmyelinated nervous system. J Neurosci : the official journal of the Society for Neuroscience 2006;26:6651–60.
[22] Khuong HT, Kumar R, Senjaya F, Grochmal J, Ivanovic A, Shakhbazau A, et al. Skin derived precursor Schwann cells improve behavioral recovery for acute and delayed nerve repair. Exp Neurol 2014;254:168–79.
[23] Grochmal J, Dhaliwal S, Stys PK, van Minnen J, Midha R. Skin-derived precursor Schwann cell myelination capacity in focal tibial demyelination. Muscle Nerve 2014;50:262–72.
[24] Shakhbazau A, Mohanty C, Kumar R, Midha R. Sensory recovery after cell therapy in peripheral nerve repair: effects of naive and skin precursor-derived Schwann cells. J Neurosurg 2014;121:423–31.
[25] Stratton JA, Shah PT, Kumar R, Stykel MG, Shapira Y, Grochmal J, et al. The immunomodulatory properties of adult skin-derived precursor Schwann cells: implications for peripheral nerve injury therapy. Eur J Neurosci 2016;43:365–75.
[26] Cong M, Shen M, Wu X, Li Y, Wang L, He Q, et al. Improvement of sensory neuron growth and survival via negatively regulating PTEN by miR-21-5p-contained small extracellular vesicles from skin precursor-derived Schwann cells. Stem Cell Res Ther 2021;12:80.
[27] Wu X, Wang L, Cong M, Shen M, He Q, Ding F, et al. Extracellular vesicles from skin precursor-derived Schwann cells promote axonal outgrowth and regeneration of motoneurons via Akt/mTOR/p70S6K pathway. Ann Transl Med 2020;8:1640.
[28] Chen Y, Shen J, Ma C, Cao M, Yan J, Liang J, et al. Skin-derived precursor Schwann cells protect SH-SY5Y cells against 6-OHDA-induced neurotoxicity by PI3K/AKT/Bcl-2 pathway. Brain Res Bull 2020;161:84–93.
[29] Yan JN, Zhang HY, Li JR, Chen Y, Jiang YC, Shen JB, et al. Schwann cells differentiated from skin-derived precursors provide neuroprotection via autophagy inhibition in a cellular model of Parkinson's disease. Neural regeneration research 2022;17:1357–63.
[30] Zhang HY, Jiang YC, Li JR, Yan JN, Wang XJ, Shen JB, et al. Neuroprotective effects of insulin-like growth factor-2 in 6-hydroxydopamine-induced cellular and mouse models of Parkinson's disease. Neural regeneration research 2023;18:1099–106.
[31] Wang T, Zeng LN, Zhu Z, Wang YH, Ding L, Luo WB, et al. Effect of lentiviral vector-mediated overexpression of hypoxia-inducible factor 1 alpha delivered by pluronic F-127 hydrogel on brachial plexus avulsion in rats. Neural regeneration research 2019;14:1069–78.
[32] Deuis JR, Dvorakova LS, Vetter I. Methods used to evaluate pain behaviors in rodents. Front Mol Neurosci 2017;10:284.
[33] Barros RSM, Santos DRD, Teixeira RKC, Araujo NP, Somensi DN, Candido AA. Anatomorphometry of the brachial plexus under high-definition system: an experimental study in rats. Acta Cir Bras 2022;37:e370206.
[34] Noland SS, Bishop AT, Spinner RJ, Shin AY. Adult traumatic brachial plexus injuries. J Am Acad Orthop Surg 2019;27:705–16.
[35] Wu KY, Spinner RJ, Shin AY. Traumatic brachial plexus injury: diagnosis and treatment. Curr Opin Neurol 2022;35:708–17.
[36] Zhang P, Lu X, Chen J, Chen Z. Schwann cells originating from skin-derived precursors promote peripheral nerve regeneration in rats. Neural regeneration research 2014;9:1696–702.
[37] Angelica-Almeida M, Casal D, Mafra M, Mascarenhas-Lemos L, Martins-Ferreira J, Ferraz-Oliveira M, et al. Brachial plexus morphology and vascular supply in the wistar rat. Acta Med Port 2013;26:243–50.
[38] Bobkiewicz A, Cwykiel J, Siemionow M. Anatomic variations of brachial and lumbosacral plexus models in different rat strains. Microsurgery 2017;37:327–33.
[39] Wang H, Wu J, Zhang X, Ding L, Zeng Q. Study of synergistic role of allogenic skin-derived precursor differentiated Schwann cells and heregulin-1beta in nerve regeneration with an acellular nerve allograft. Neurochem Int 2016;97:146–53.
[40] Song L, Guo Q, Guo J, Xu X, Xu K, Li Y, et al. Brachial plexus bridging with specific extracellular matrix-modified chitosan/silk scaffold: a new expand of tissue engineered nerve graft. J Neural Eng 2022;19.
[41] Qu WR, Zhu Z, Liu J, Song DB, Tian H, Chen BP, et al. Interaction between Schwann cells and other cells during repair of peripheral nerve injury. Neural regeneration research 2021;16:93–8.
[42] Moeinabadi-Bidgoli K, Babajani A, Yazdanpanah G, Farhadihosseinabadi B, Jamshidi E, Bahrami S, et al. Translational insights into stem cell preconditioning: from molecular mechanisms to preclinical applications. Biomed Pharmacother 2021;142:112026.
[43] Daines JM, Schellhardt L, Wood MD. The role of the IL-4 signaling pathway in traumatic nerve injuries. Neurorehabilitation Neural Repair 2021;35:431–43.
[44] Gunner G, Cheadle L, Johnson KM, Ayata P, Badimon A, Mondo E, et al. Sensory lesioning induces microglial synapse elimination via ADAM10 and fractalkine signaling. Nat Neurosci 2019;22:1075–88.
[45] Subbarayan MS, Joly-Amado A, Bickford PC, Nash KR. CX3CL1/CX3CR1 signaling targets for the treatment of neurodegenerative diseases. Pharmacol Therapeut 2022;231:107989.
[46] Guha S, Paidi RK, Goswami S, Saha P, Biswas SC. ICAM-1 protects neurons against Amyloid-beta and improves cognitive behaviors in 5xFAD mice by inhibiting NF-kappaB. Brain Behav Immun 2022;100:194–210.
[47] Fang S, Tang H, Li MZ, Chu JJ, Yin ZS, Jia QY. Identification of the CCL2 PI3K/Akt axis involved in autophagy and apoptosis after spinal cord injury. Metab Brain Dis 2023;38:1335–49.
[48] Wang L, Li J, Wang Y, Ge C, Huang Q, Li L, et al. Dan-Deng-Tong-Nao softgel capsule promotes angiogenesis of cerebral microvasculature to protect cerebral ischemia reperfusion injury via activating HIF-1alpha-VEGFA-Notch1 signaling pathway. Phytomedicine 2023;118:154966.
[49] Lund MC, Ellman DG, Nielsen PV, Raffaele S, Fumagalli M, Guzman R, et al. Selective inhibition of soluble tumor necrosis factor alters the neuroinflammatory response following moderate spinal cord injury in mice. Biology 2023;12.
[50] Wong R, Smith CJ, Allan SM, Pinteaux E. Preconditioning with interleukin-1 alpha is required for the neuroprotective properties of mesenchymal stem cells after ischaemic stroke in mice. J Cerebr Blood Flow Metabol 2023;43:2040–8.
[51] Xia X, He X, Zhao T, Yang J, Bi Z, Fu Q, et al. Inhibiting mtDNA-STING-NLRP3/IL-1beta axis-mediated neutrophil infiltration protects neurons in Alzheimer's disease. Cell Prolif 2023:e13529.
[52] Guo XY, Duan FX, Chen J, Wang Y, Wang R, Shen L, et al. Subcutaneous administration of PDGF-AA improves the functional recovery after spinal cord injury. Front Neurosci 2019;13:6.
[53] Perez-Gutierrez L, Ferrara N. Biology and therapeutic targeting of vascular endothelial growth factor A. Nat Rev Mol Cell Biol 2023;24:816–34.
[54] Molnar K, Nogradi B, Kristof R, Meszaros A, Pajer K, Siklos L, et al. Motoneuronal inflammasome activation triggers excessive neuroinflammation and impedes regeneration after sciatic nerve injury. J Neuroinflammation 2022;19:68.
[55] Zigmond RE, Echevarria FD. Macrophage biology in the peripheral nervous system after injury. Prog Neurobiol 2019;173:102–21.
[56] Msheik Z, El Massry M, Rovini A, Billet F, Desmouliere A. The macrophage: a key player in the pathophysiology of peripheral neuropathies. J Neuroinflammation 2022;19:97.
[57] Feng R, Muraleedharan Saraswathy V, Mokalled MH, Cavalli V. Self-renewing macrophages in dorsal root ganglia contribute to promote nerve regeneration. Proc Natl Acad Sci USA 2023;120:e2215906120.
[58] Ross SH, Cantrell DA. Signaling and function of interleukin-2 in T lymphocytes. Annu Rev Immunol 2018;36:411–33.
[59] Bassler K, Schulte-Schrepping J, Warnat-Herresthal S, Aschenbrenner AC, Schultze JL. The myeloid cell compartment-cell by cell. Annu Rev Immunol 2019;37:269–93.
[60] Zhu H, Wang Z, Yu J, Yang X, He F, Liu Z, et al. Role and mechanisms of cytokines in the secondary brain injury after intracerebral hemorrhage. Prog Neurobiol 2019;178:101610.
[61] Buttner R, Schulz A, Reuter M, Akula AK, Mindos T, Carlstedt A, et al. Inflammaging impairs peripheral nerve maintenance and regeneration. Aging Cell 2018;17:e12833.
[62] Rose-John S, Jenkins BJ, Garbers C, Moll JM, Scheller J. Targeting IL-6 trans-signalling: past, present and future prospects. Nat Rev Immunol 2023:1–16.
[63] Balakrishnan A, Belfiore L, Chu TH, Fleming T, Midha R, Biernaskie J, et al. Insights into the role and potential of Schwann cells for peripheral nerve repair from studies of development and injury. Front Mol Neurosci 2020;13:608442.
[64] Jessen KR, Mirsky R, Lloyd AC. Schwann cells: development and role in nerve repair. Cold Spring Harbor Perspect Biol 2015;7:a020487.
[65] Saio S, Konishi K, Hohjoh H, Tamura Y, Masutani T, Iddamalgoda A, et al. Extracellular environment-controlled angiogenesis, and potential application for peripheral nerve regeneration. Int J Mol Sci 2021;22.
[66] Min Q, Parkinson DB, Dun XP. Migrating Schwann cells direct axon regeneration within the peripheral nerve bridge. Glia 2021;69:235–54.
[67] Yang XP, Mattagajasingh S, Su S, Chen G, Cai Z, Fox-Talbot K, et al. Fractalkine upregulates intercellular adhesion molecule-1 in endothelial cells through CX3CR1 and the Jak Stat5 pathway. Circ Res 2007;101:1001–8.

[68] Suzuki T, Kadoya K, Endo T, Iwasaki N. Molecular and regenerative characterization of repair and non-repair Schwann cells. Cell Mol Neurobiol 2023;43:2165–78.
[69] Zhu HY, Bai WD, Liu JQ, Zheng Z, Guan H, Zhou Q, et al. Up-regulation of FGFBP1 signaling contributes to miR-146a-induced angiogenesis in human umbilical vein endothelial cells. Sci Rep 2016;6:25272.
[70] Ribatti D, Tamma R, Annese T. The role of vascular niche and endothelial cells in organogenesis and regeneration. Exp Cell Res 2021;398:112398.
[71] Cattin AL, Burden JJ, Van Emmenis L, Mackenzie FE, Hoving JJ, Garcia Calavia N, et al. Macrophage-induced blood vessels guide Schwann cell-mediated regeneration of peripheral nerves. Cell 2015;162:1127–39.
[72] Li M, Cheng X, Feng S, Zhu H, Lu P, Zhang P, et al. Skin precursor-derived Schwann cells accelerate in vivo prevascularization of tissue-engineered nerves to promote peripheral nerve regeneration. Glia 2023;71:1755–69.
[73] Stothert AR, Kaur T. Innate immunity to spiral ganglion neuron loss: a neuroprotective role of fractalkine signaling in injured cochlea. Front Cell Neurosci 2021;15:694292.
[74] Buffolo F, Petrosino V, Albini M, Moschetta M, Carlini F, Floss T, et al. Neuroinflammation induces synaptic scaling through IL-1beta-mediated activation of the transcriptional repressor REST/NRSF. Cell Death Dis 2021;12:180.
[75] Ng T, Hor CH, Chew B, Zhao J, Zhong Z, Ryu JR, et al. Neuropilin 2 signaling is involved in cell positioning of adult-born neurons through glycogen synthase kinase-3beta (GSK3beta). J Biol Chem 2016;291:25088–95.
[76] Tan Z, Qin S, Yuan Y, Hu X, Huang X, Liu H, et al. NOTCH1 signaling regulates the latent neurogenic program in adult reactive astrocytes after spinal cord injury. Theranostics 2022;12:4548–63.
[77] Robert AW, Azevedo Gomes F, Rode MP, Marques da Silva M, Veleirinho M, Maraschin M, et al. The skin regeneration potential of a pro-angiogenic secretome from human skin-derived multipotent stromal cells. J Tissue Eng 2019;10:2041731419833391.
[78] Takahama S, Adetunji MO, Zhao T, Chen S, Li W, Tomarev SI. Retinal astrocytes and GABAergic wide-field amacrine cells express PDGFRalpha: connection to retinal ganglion cell neuroprotection by PDGF-AA. Invest Ophthalmol Vis Sci 2017;58:4703–11.
[79] Daneshmandi L, Shah S, Jafari T, Bhattacharjee M, Momah D, Saveh-Shemshaki N, et al. Emergence of the stem cell secretome in regenerative engineering. Trends Biotechnol 2020;38:1373–84.
[80] Eggers R, de Winter F, Tannemaat MR, Malessy MJA, Verhaagen J. GDNF gene therapy to repair the injured peripheral nerve. Front Bioeng Biotechnol 2020;8:583184.